Seismic metamaterial barriers for ground vibration mitigation in railways considering the train-track-soil dynamic interactions

Li, Ting; Su, Qian; Kaewunruen, Sakdirat

Seismic metamaterial barriers for ground vibration mitigation in railways considering the train-track-soil dynamic interactions

Ting Li[a,b,c], Qian Su[a,b], Sakdirat Kaewunruen[c,*]

[a] *School of Civil Engineering, Southwest Jiaotong University, Chengdu 610031, China*

[b] *Key Laboratory of High-Speed Railway Engineering, Ministry of Education, Southwest Jiaotong University, Chengdu 610031, China*

[c] *School of Engineering, University of Birmingham, Birmingham B15 2TT, UK*

[*]Correspondence should be addressed to Sakdirat Kaewunruen (s.kaewunruen@bham.ac.uk).

Abstract: With the rapid development of high speed rail system, ground vibration mitigation solutions are desperately needed. Based on the concepts of phononic crystals, seismic metamaterial, which is a novel vibration mitigation method, can theoretically yield excellent performance in shielding dynamic propagation waves in broad frequency bands. However, the application of seismic metamaterials in railway-induced vibration mitigation is a recent and ongoing topic. Therefore, this study aims to create new contribution towards a better understanding into the mitigation effects by seismic metamaterials for railway-induced ground vibrations. The seismic metamaterials are made of an array of concrete inclusions in this study. The dispersion theory for seismic metamaterials is proposed for analyzing the theoretical band gaps. A 3D coupled train-track-soil interaction model is also developed based on the multi-body simulation principle, finite element theory, and perfectly matched layers method using LS-DYNA. The dimensions of seismic metamaterials are determined based on the dominant frequencies of vibration accelerations in natural ground. When the seismic metamaterials are adopted in railway ground, the vibration responses are investigated in both time and frequency domains to illustrate the mitigation effects. Finally, the numbers of inclusions, initial distances, and train speeds are changed to investigate their influences on shielding effects. The insight from this study provides a new and better understanding of attenuating ground vibrations using seismic metamaterials in high speed railways.

Keywords: seismic metamaterials; band gap; ground vibration mitigation; train-track-soil interactions

1. Introduction

High-speed rail is undergoing rapid development with the demand to increase operating train speeds all over the world [1-3]. Numerous high-speed trains with a maximum operating speed of 380 km/h are traveling in China. The demand to elevate train speed brings new challenges for high-speed rail infrastructures, especially for the ground-borne vibrations. Train-induced ground vibrations can negatively affect surrounding residents, buildings, tunnels, drainage systems, overhead wiring structures, and so on [4, 5, 34, 35, 36]. Effective and efficient vibration mitigation solutions are desperately needed for high speed rail networks.

Considerable efforts have been made for the mitigation of the railway-induced vibrations. Active isolation techniques, such as floating slab tracks, softer rail pads and resilient wheels, have been investigated to attenuate railway vibrations from sources [6, 7]. Mitigation measures can also be applied to the propagation paths of dynamic waves in soils, termed as passive isolation. The passive isolation solutions can be open trenches, in-filled trenches, sheet pile walls, and so on [8, 9]. Although these solutions exhibit good vibration attenuation performance, there are some difficulties in practice when these structures are constructed in soils. For instance, the stability of opening holes is a concern, and the trench is challenging to be built in unstable and soft soils [10]. As a type of passive isolation, seismic metamaterial (SMM), which is a recently proposed solution based on the concepts of phononic crystals, is receiving increasing attention [11, 12].

The term metamaterials emerged from electromagnetism in a nano-scale world. During the last several decades, the investigation of SMM in attenuating all types of waves, such as ultrasound, acoustic, elastic, electromagnetic waves and even thermal fluctuations, has drawn considerable interest from a large number of scientists and engineers [13-15]. In engineering, SMM is a type of unique material designed and built to acquire one (or more than one) property not found in naturally occurring materials, such as a negative index of refraction [16]. The inclusions of SMM are normally designed using a combination of multiple elements arranged in repeating patterns. Due to the periodicity of the structure, the filtering effect of the SMM provides the possibility to attenuate the vibration in certain frequency bands. When the

frequencies of the incident waves fall into a blind zone, termed as band gap, the waves can be blocked in any directions, so that they cannot propagate anymore [17, 18].

With the development of the SMM field, many types of SMM have emerged with a decade of research. Based on the literature review, Brule et al. [14] proposed four categories of the SMM: seismic soil-metamaterials [19, 20], buried mass-resonators [21], above-surface resonators [11, 12], and auxetic materials [22]. The seismic-soil metamaterials are quite convenient to be adopted in soils. Brule et al. [23, 24] designed the SMM with a grid of cylindrical holes in soils and carried out large-scale field tests to investigate the Bragg's effect and distribution of energies in soils. The band gap of such kind of SMM is around 50 Hz. Miniaci et al. [25] investigated the parameters that affect band gaps of SMM by carrying out a numerical analysis with large-scale mechanical metamaterials, which are made of cavities or rubber/steel/concrete-infilled inclusions. Numerous scholars have also investigated the band gaps of SMM by adopting an array of piles, which possess an excellent performance in mitigating vibrations [19, 20, 26]. Despite the recent advances in this field, the SMM is mostly designed for shielding seismic waves from earthquakes. Kaewunruen et al. [16] were the first to evaluate the railway-induced ground vibration mitigation using SMM with the aim of life-cycle performance analysis, indicating that the SMM has a high possibility to be used as wave barriers in railway ground. Thompson el al. [27] also proposed that the application of SMM in attenuating railway-induced ground vibrations is an open question and needs further investigations.

Considering the vibration mitigation by SMM is recent, and the related research is still ongoing, this study aims to give a contribution of understanding the mitigation effects of SMM adopted in railways by carrying out a numerical analysis. An array of piles is chosen to be SMM in this study as the pile inclusions are the simplest way to be constructed in practice. The dispersion theory for SMM is first introduced to find out the theoretical band gaps. Then, a 3D coupled train-track-soil interaction model is developed using LS-DYNA to investigate the ground vibration mitigation effects using SMM. This study could bring an insightful and new understanding of the vibration mitigation by the novel solution of SMM in high-speed railways.

2. Dispersion theory for seismic metamaterials

The dispersion characteristics of the seismic metamaterial (SMM) can theoretically demonstrate the ground vibration mitigation components in frequency domain since the dispersion relation of the SMM illustrates the modes of wave propagation with passbands and band gaps, where seismic waves cannot pass. The dispersion theory for SMM is thus firstly introduced.

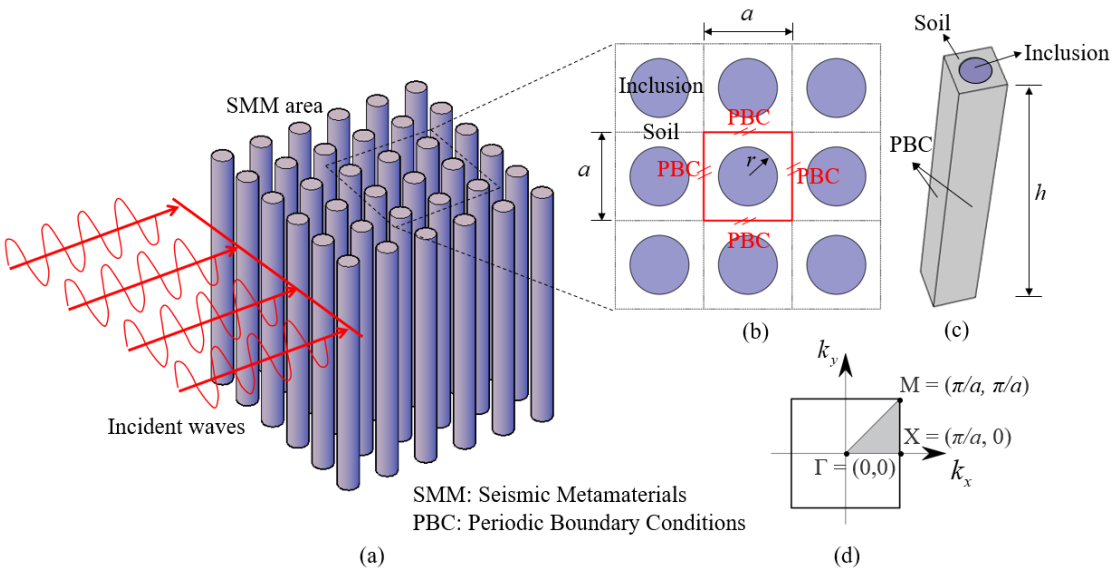

Figure 1 Schematic representation of the SMM (a) Periodic array of barriers (b) Plan view (c) Unit cell in Comsol Multiphysics (d) The first Brillouin zone with the irreducible part (light grey triangle of vertices Γ-X-M)

As shown in Figure 1 (a), the SMM appears typically as a periodic array of barriers to interact with the incident waves to mitigate the vibration responses. The concrete piles with circular sections are considered as inclusions of the SMM in this study. Both soil and inclusion are assumed to be homogenous, linearly elastic, and perfectly bonded materials [20].

2.1 Wave equation

For the isotropic, linear elastic medium without considering of damping and body force, the governing equation of waves propagating in periodic structures is written as follows [20]:

$$\rho \frac{\partial^2 \mathbf{u}}{\partial t^2} - \nabla \cdot c \nabla \mathbf{u} = 0 \tag{1}$$

where ρ is the mass density, $\mathbf{u}$ is the displacement vector, t is time, ∇ is differential operator, and c is the elastic constant.

2.2 Floquet-Bloch theory and periodic boundary conditions

Since the SMM is a periodic system, a unit cell with the lattice constant a can be studied for the dispersion relations by applying periodic boundary, as shown in Figure 1 (b) and (c). The Floquet-Bloch theory was originally developed to solve the differential equations of wave-like particles in physical sciences, and it is adopted here to study the behavior of wave propagation in the periodic unit cell [12]. According to the Floquet-Bloch theory, the displacement vector in Eq. (1) can be written as:

$$\mathbf{u}(\mathbf{r}, t) = e^{i(\mathbf{k}\cdot\mathbf{r} - \omega t)} \mathbf{u}_{\mathbf{k}}(\mathbf{r}) \tag{2}$$

where $\mathbf{k}$ is the Floquet-Bloch wave vector in the first Brillouin zone [28], $\mathbf{r}$ is the coordinate vector, ω is the angular frequency, and $\mathbf{u}_{\mathbf{k}}(\mathbf{r})$ is a modulation function of the displacement vector. The modulation function is a periodic function defined in the unit cell:

$$\mathbf{u}_{\mathbf{k}}(\mathbf{r}) = \mathbf{u}_{\mathbf{k}}(\mathbf{r} + \mathbf{a}) \tag{3}$$

where $\mathbf{a}$ is the lattice constant vector, $\mathbf{a} = (a_x, a_y)$. In this study, the inclusions are arranged in the shape of square, therefore $a_x = a_y = a$.

Substituting Eq. (3) into Eq. (2), the periodic boundary conditions (PBC) for a unit cell are obtained,

$$\mathbf{u}_{\mathbf{k}}(\mathbf{r} + \mathbf{a}, t) = e^{i\mathbf{k}\cdot\mathbf{a}} \mathbf{u}_{\mathbf{k}}(\mathbf{r}, t) \tag{4}$$

2.3 Dispersion equation and solutions

By combining the Eq. (1) and Eq. (4), the dispersion relation of a periodic system can be transferred into an eigenvalue equation:

$$(\mathbf{\Omega(k)} - \omega^2\mathbf{M}) \cdot \mathbf{u} = \mathbf{0} \tag{5}$$

where $\mathbf{\Omega(k)}$ and $\mathbf{M}$ are the stiffness and mass matrices of the unit cell, respectively. The dispersion relation is an implicit function between the wave vector $\mathbf{k}$ and eigenfrequency ω. In order to consider all the wave propagation modes, the wave vector $\mathbf{k}$ should be changed across the boundary of the first irreducible Brillouin zone (Γ-X-M) [28], as shown in Figure 1 (d). For a wave vector where no frequency exists, it is termed the band gap, where no wave propagation appears.

The commercial software Comsol Multiphysics is used to solve the eigenvalue equation and dispersion relation. It is noted that the soil and inclusion are normally modeled with a large depth h to simulate the infinite thickness of the unit cell [29]. The PBC is applied to all vertical sides of the unit cell, while a fixed boundary is adopted on the bottom surface. The eigenfrequency studies and complex boundaries as Eq. (4) are chosen in the software. The eigenfrequencies are obtained by sweeping wave vectors in the first irreducible Brillouin zone, and the dispersion relation of the SMM is obtained by solving the eigenvalue equation.

3. Modeling of the train-track-soil dynamic interactions

Although the dispersion relation of the SMM illustrates the characteristics of seismic wave propagations, there are lots of assumptions with ideal conditions when the theoretical dispersion relation is obtained. The ground vibration mitigation effect using SMM in high-speed railways is unknown in practice. In order to investigate the ground vibration attenuation level using SMM in railways, a novel 3D coupled train-track-soil model is developed in LS-DYNA. The high-speed train is simulated based on the multi-body simulation (MBS) principle, and the slab track is developed based on the finite element modeling (FEM) theory. The soils and the SMM are simulated based on the FEM theory together with the Perfectly Matched Layers (PML) method.

3.1 Modeling of the high-speed train and slab track

A commonly operated Chinese high-speed train, the China Railway High-speed (CRH)

380 Electric Multiple Unit (EMU) train, is simulated in this model. The vehicle consists of one car body, two bogies, four wheelsets, and two stage-suspension systems, as shown in Figure 2. The car body, bogies, and wheelsets are simplified as the rigid-bodies using shell and beam elements. The springs and dashpots connect these multi-rigid-bodies. As the vertical vibration is the primary excitation to the infrastructures, the vertical degrees of freedom (DOF) of the vehicle are considered in this model. The vehicle has 10 DOF, including the vertical and pitch motion of car body (Z_c, β_c), the vertical and pitch motion of bogies (Z_{bi}, β_{bi} $i = 1,2$), and the vertical motion of wheelsets (Z_{wi} $i = 1,...,4$).

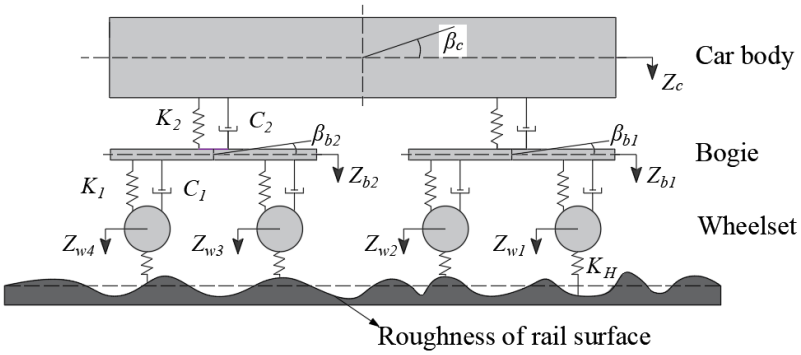

Figure 2 Simulation of the vehicle

The China Railway Track System (CRTS) II slab track is adopted in this model. It consists of rail, rail pads, concrete slab, cement asphalt (CA) mortar layer, and concrete base [30]. The rail is simulated as the Euler beam, which is supported by the discrete springs and dashpots to represent the rail pads. This beam model may yield around 5-8% of discrepancy when compared with Timoshenko beam theory. However, this discrepancy is acceptable for the purpose of track substructure vibration analysis since the vibrations at lower layers of tracks are already suppressed by the track structure [2]. The concrete slab, CA mortar, and concrete base are simulated as solid elements with brick mesh.

The contact between wheel and rail is simulated based on the Hertz contact theory by using keywords: *Rail_Track and *Rail_Train. LS-DYNA can automatically calculate the wheel-rail contact force based on the following equation:

$$F = K_H \times (Z_w - Z_r - \delta) \tag{6}$$

where K_H is the vertical stiffness of the wheel-rail contact spring, K_H =1.325×10^9 N/m in this study [31]; Z_w is the vertical displacement of the wheel; Z_r is the vertical displacement of the rail; and δ is the roughness of rail surface. The Germany high-speed low disturbance

irregularity is used to excite the wheel-rail contact. The power spectrum density (PSD) function of the roughness is calculated as follows:

$$S_v(\Omega) = \frac{A_v \Omega_c^2}{(\Omega^2 + \Omega_r^2)(\Omega^2 + \Omega_c^2)} \tag{7}$$

where A_v is the roughness constant ($A_v = 4.032 \times 10^{-7}$ m$^2 \cdot$ Rad/m); Ω_c and Ω_r are the cutoff frequency ($\Omega_c = 0.8246$ rad/m , $\Omega_r = 0.0206$ rad/m); and Ω is the spatial frequency of the roughness. The PSD function can be transformed into vertical roughness along the longitudinal distance of the track using a time-frequency transformation technique, as shown in Figure 3.

The material properties of the CRH380 EMU Train and CRTS II slab track can be found from [4] and [5].

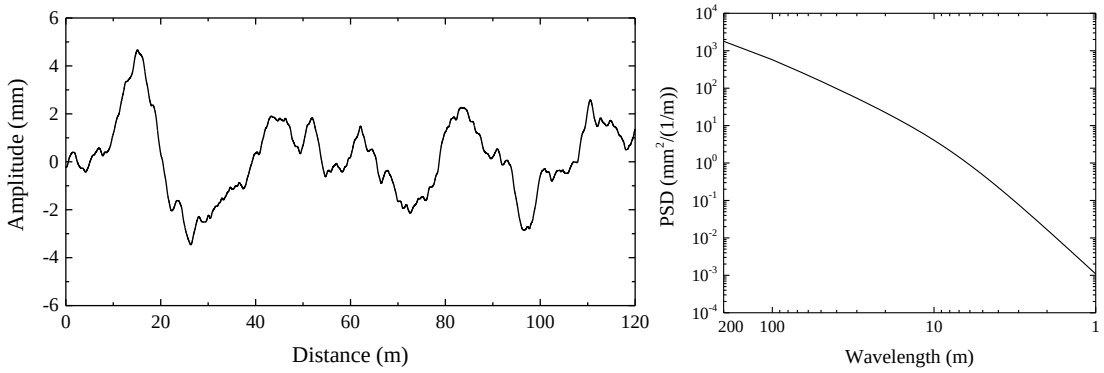

(a) Roughness with distance (b) PSD with wavelength

Figure 3 The roughness of rail surface

3.2 Modeling of soils and seismic metamaterials

Soils are composed of subgrade soils and ground soils. There are three layers in subgrade: surface layer with a depth of 0.4 m, bottom layer with a depth of 2.3 m, and subgrade body with a depth of 2.4 m [4]. The ground consists of one layer with a depth of 15 m [17]. These soils are simulated as viscoelastic material using solid elements. The mesh of brick is used to simulate a large portion of soils, and some adaptive shapes like wedge and cylinder are used to simulate the soils near SMM.

The concrete inclusion of SMM is simulated using solid elements in this model. Note that infinite periodic structures do not exist in practice, therefore thirty six (6×6) inclusions are constructed to demonstrate the periodic characteristics of the SMM in the model. The

inclusions are simulated by solid elements. The dimensions of inclusions will be discussed in the following parts.

As the most efficient infinite boundary, perfectly matched layers (PML) method is used to prevent spurious wave reflections from the truncated boundary [32, 33, 34, 35, 36, 37].

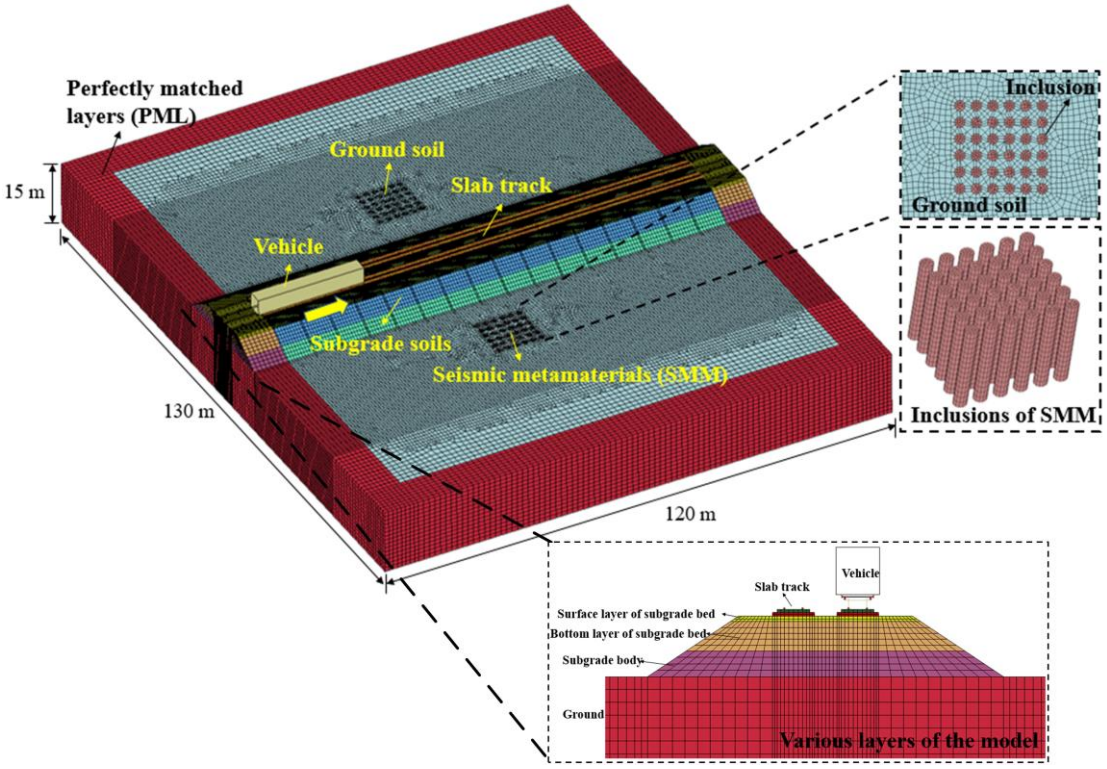

Figure 4 The 3D coupled train-track-soil model in LS-DYNA

Table 1 Material properties of soils and SMM

Components		Density (kg/m^3)	Modulus of elasticity (MPa)	Poisson's ratio	Rayleigh damping
Subgrade [4]	Surface layer	2300	200	0.25	α=0 β=0.0002
	Bottom layer	1950	150	0.35	
	Subgrade body	2100	110	0.3	
Ground [17]	Ground soft soil	1800	20	0.3	
SMM [17]	Concrete inclusions	2500	40000	0.2	-

Figure 4 illustrates the coupled train-track-soil model in LS-DYNA. The dimension of the ground is 120 m × 130 m × 15 m. A double-track railway, which is commonly constructed

in China, is simulated in the model. Note that the SMM is built at the right side of the railway, while the left side of ground has the same mesh but with ground soils inside. The materials properties of the soils and SMM are shown in Table 1.

3.3 Numerical solution

The vehicle is set to travel at a constant speed over the rail after the dynamic relaxation. The explicit central difference method is used to integrate the equations of motion of the coupled train-track-soil system by LS-DYNA with a time step of 1.23×10^{-5} s.

4. Model validation

The concrete and steel inclusions of the SMM are adopted to validate the proposed dispersion theory. The material properties and dimensions of the two types of inclusions are shown in table 2. The boundary conditions are set according to previous references [17, 18].

Table 2 Material properties and dimensions of two types of inclusions of SMM

SMM		Density (kg/m^3)	Modulus of elasticity (MPa)	Poisson's ratio	a (m)	r (m)	h (m)
Concrete inclusion [17]	Concrete	2500	40000	0.2	3	1.2	6
	Soil	1800	20	0.3			
Steel inclusion [18]	Steel	7850	200000	0.33	2	0.6	15+5 (bedrock)
	Soil	1800	153	0.3			

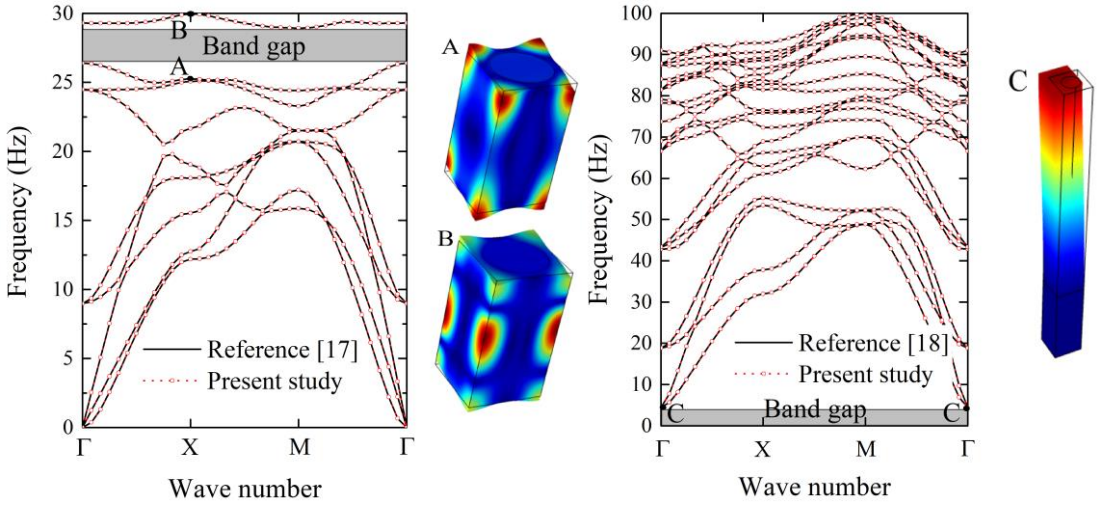

(a) (b)

Figure 5 Dispersion relations and mode shapes of SMM (a) Concrete inclusion (b) Steel inclusion

The dispersion relation and mode shapes of the concrete and steel inclusions of the SMM are shown in Figure 5. The concrete inclusion has a band gap of 26-29 Hz, while the steel inclusion shows a band gap of 0-4.5 Hz, indicating that the dynamic waves will be theoretically attenuated at these frequencies within band gaps. The dispersion curves obtained from this study exhibit a very good agreement with previous references [17, 18]. Also, the mode shapes are quite similar to those from references [17, 18]. Therefore, the dispersion theory proposed in this study can illustrate the theoretical dispersion characteristics of the SMM.

The 3D coupled train-track-soil interaction model has been validated in previous studies, and the validation results can be found from [4] and [5].

5. Ground vibration analysis

The pronounced frequency components should be mitigated in railways, and they correspond to the theoretical band gap of SMM. However, the band gaps vary with the dimensions of SMM. In order to determine the lattice constant and radius of the inclusions, the dominant frequencies of natural ground are first investigated from the coupled train-track-soil interaction model. The dimensions of the SMM are thus determined based on the pronounced frequency components of natural ground. The vibration responses from the models with and without SMM are then compared in time and frequency domain to illustrate the ground vibration mitigation effects using SMM in high-speed railways.

5.1 Dimensions of seismic metamaterials

The frequency components of natural ground are obtained by applying Fast Fourier Transformation (FFT) to time history of vibration accelerations when the train travels with a speed of 380 km/h. Figure 6 illustrates the frequency distribution of railway ground without SMM.

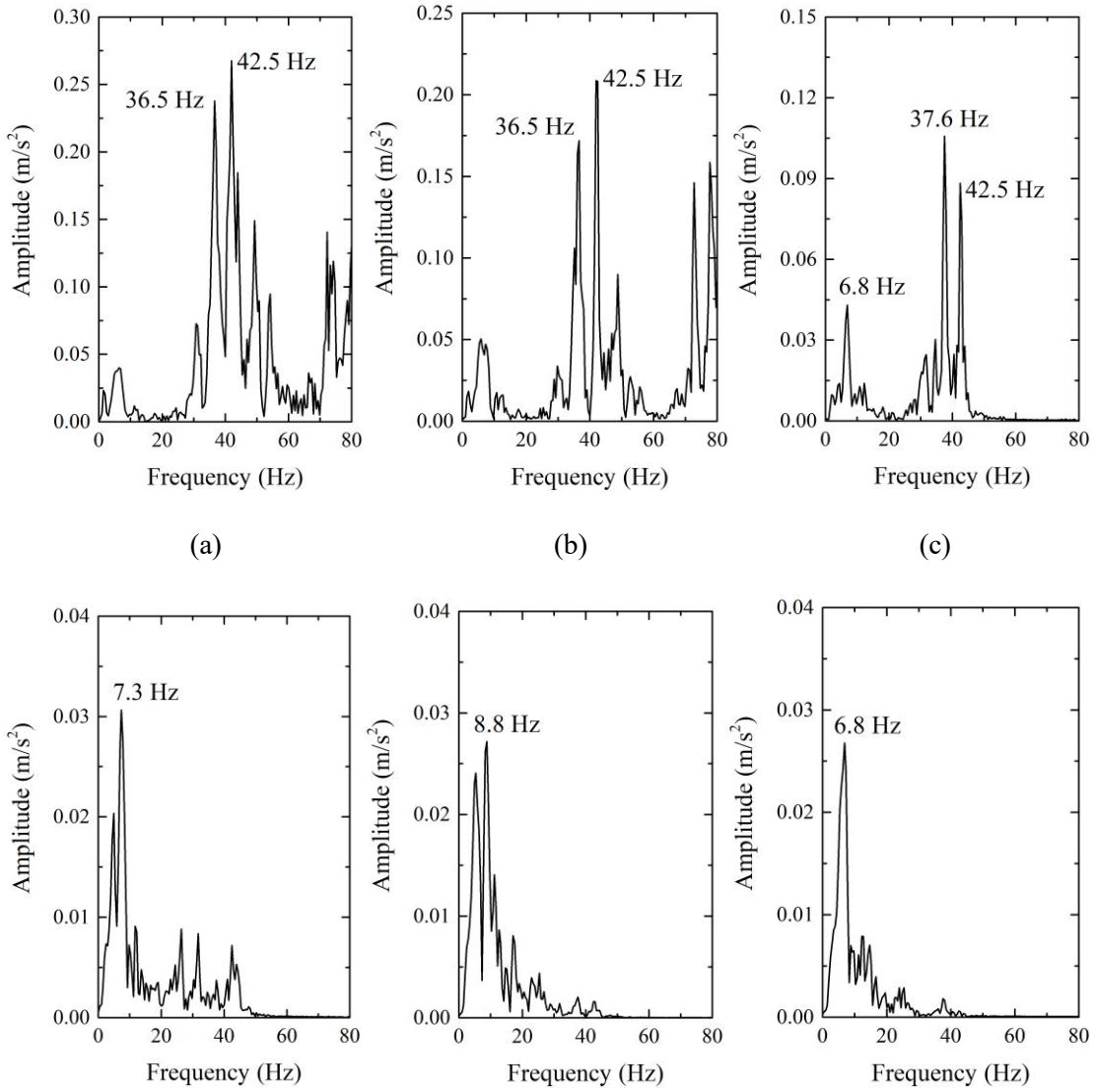

Figure 6 Frequency distribution of natural ground with varied lateral distances (a) 4.3 m (b) 11.4 m (c) 18.4 m (d) 24.4 m (e) 30 m (f) 36.4 m

When the soil is relatively close to the railway track (≤ 18.4 m), the pronounced frequencies are distributed in 36.5 - 42.5 Hz, as shown in Figure 6 (a), (b) and (c). It is likely that the repeated actions of wheelsets induce the component of 42.5 Hz as the theoretical frequency is $f_1 = v / l_1 = 380 / 3.6 / 2.5 = 42.2\,\text{Hz}$ (l_1 is the distance between two wheelsets). The resonance of track irregularities might induce the 36.5 Hz or 37.6 Hz. When the distance is longer than 18.4 m, the lower frequencies become dominant. The pronounced frequencies are in the range of 6.8 – 8.8 Hz, as shown in Figure 6 (d), (e) and (f). The repeated actions of bogies likely induce this frequency since the theoretical frequency is

$f_2 = v / l_2 = 380 / 3.6 / 17.5 = 6.03\,\text{Hz}$ (l_2 is the distance between two bogies). Small differences between frequency components, such as 6.8 Hz and 8.8 Hz, are likely caused by different mesh sizes. Note that the environmental structures and residents are normally located at distances longer than 18.4 m, the attenuated frequencies should be lower than 9 Hz in this case.

The concrete inclusions are adopted in high-speed railways in this study. The depth of the SMM is 15 m to simulate the deep thickness according to [17]. Based on the characteristics of concrete inclusions from [17], the SMM exhibits a theoretical band gap with 0 - 9.1 Hz when the lattice constant is 2 m and radius of inclusions is 0.65 m, as shown in Figure 7. Therefore, the SMM with the selected dimensions can theoretically attenuate the dynamic vibrations with frequencies lower than 9.1 Hz, which is in line with the target frequencies obtained from the coupled train-track-soil interaction model. Also, the mode shapes at Point A and Point B exhibit a shear-like mode [18], indicating that the SMM can attenuate shear waves in railways. In short, the SMM with lattice constant of 2 m and radius of 0.65 m and depth of 15 m is adopted in the coupled train-track-soil interaction model to investigate the ground vibration mitigation effect in high-speed railways.

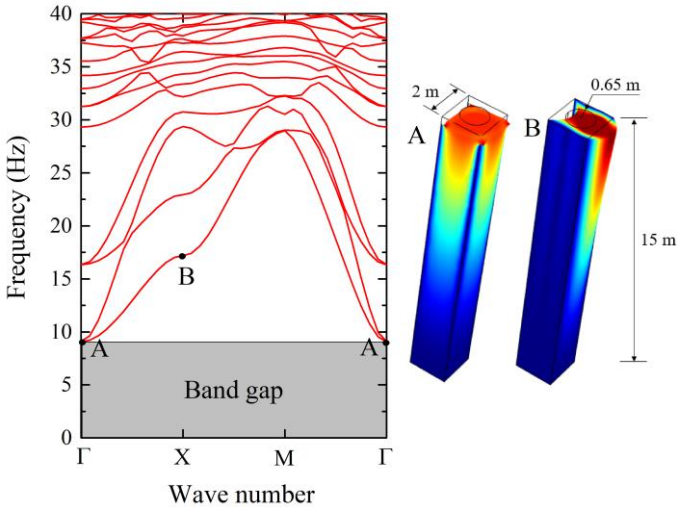

Figure 7 Dispersion relation and mode shapes of the SMM adopted in railways

5.2 Mitigation effect using seismic metamaterials

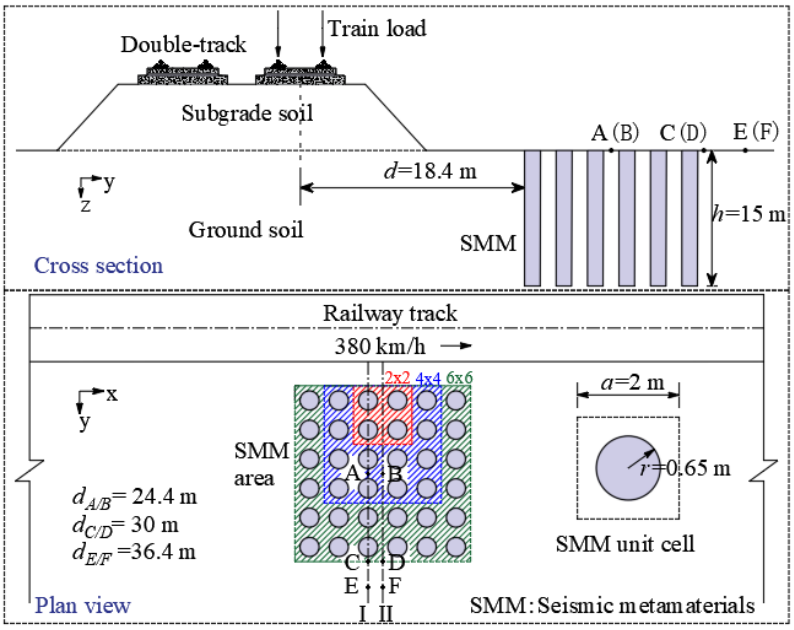

Figure 8 Distribution of the SMM and monitor points in railways

The SMM with 36 (6×6) concrete inclusions is adopted in the railway ground, as illustrated in Figure 8. The initial distance (d) between the front edge of SMM and the center line of the right track is 18.4 m. The lateral distance along with two lines (Line I and Line II) are chosen as monitoring locations in this railway. Six points (Point A, B, C, D, E, and F) with different lateral distances are also selected as key points. The vibration responses from these monitoring locations are compared in both time and frequency domains.

5.2.1 Time domain analysis

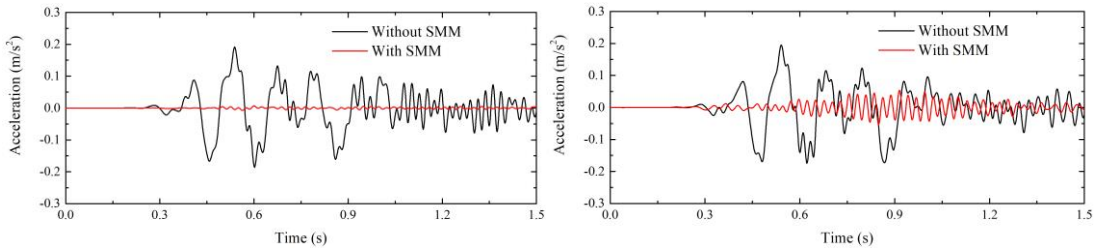

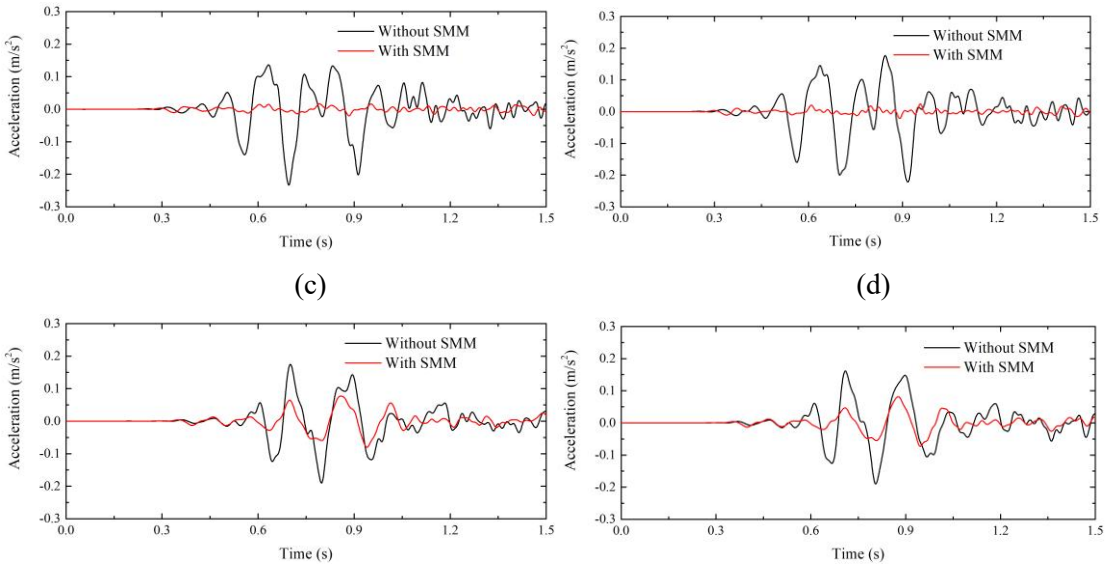

Figure 9 Time history of vibration accelerations (a) Point A (b) Point B (c) Point C (d) Point D (e) Point E (f) Point F

Figure 9 shows the time history curves of the vibration accelerations at six key points in this railway. The SMM exhibits a significant vibration mitigation effect as the amplitudes of vibration accelerations with SMM are much lower than those without SMM. The attenuation effect is quite similar at 24.4 m (A and B) and 30 m (C and D). But the mitigation effect weakens at 36.4 m since Point E and F are located behind the SMM area.

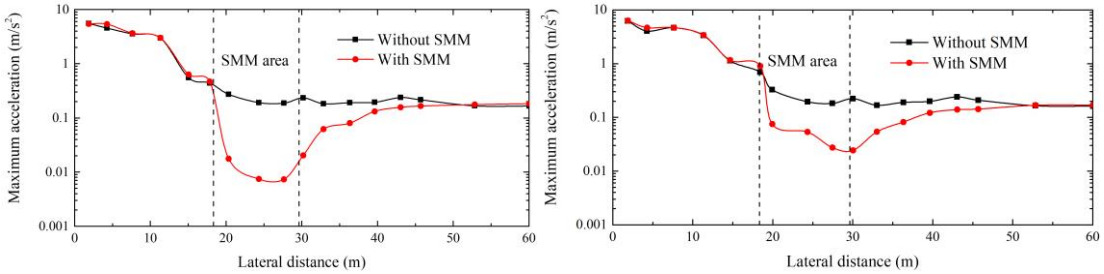

Figure 10 Maximum acceleration with lateral distance (a) Line I (b) Line II

The maximum accelerations along with Line I and Line II are shown in Figure 10. When the distance is shorter than 18.4 m, which is the front edge of SMM area, the maximum accelerations with and without SMM exhibit no evident differences. However, when the dynamic waves approach the SMM area, the SMM exhibits a significant vibration mitigation effect. The maximum acceleration achieves a maximum reduction of 96% from 0.19 m/s^2 to 0.007 m/s^2 in Line I, and 91% from 0.22 m/s^2 to 0.02 m/s^2 in Line II. Globally, the reduction

effect along with Line I is better than that along with Line II. The significant vibration mitigation effect is mainly induced by the higher modulus and density that SMM possesses. When the distance is longer than the back edge of SMM area, the SMM can still attenuate the vibration accelerations. And the maximum accelerations converge to the same magnitude when the distance is longer than 50 m. It is noted that when the SMM is adopted in the railway, the maximum acceleration at 18.4 m is a little bit higher than that without SMM. It is likely that the dynamic waves reflect when they approach the barriers, resulting in higher ground vibration response at the front edge of SMM area.

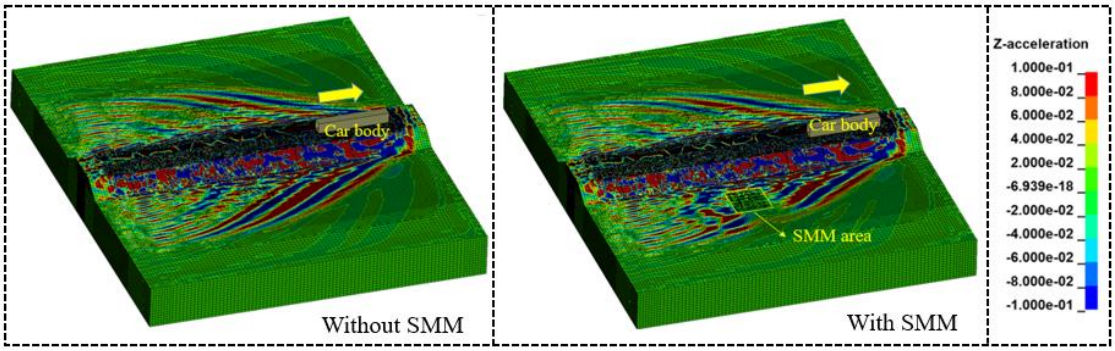

(a)

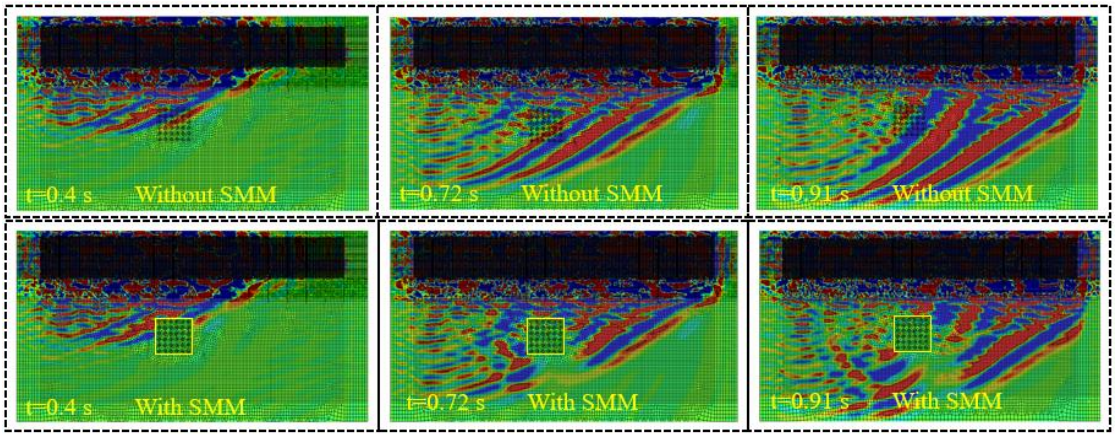

(b)

Figure 11 Contours of the ground vibration acceleration (a) 3D view (b) plan view

Figure 11 illustrates the contours of the ground vibration acceleration with two cases: with and without SMM. Note that the acceleration values are set between -0.1 m/s^2 and 0.1 m/s^2 in order to present a clear propagation path of dynamic waves. The Mach cone phenomenon, which is analogous to a boat moving through the water, can be observed from the 3D view in both cases. But the SMM affects the propagations of dynamic waves, as

shown in Figure 11 (a). Figure 11 (b) illustrates the distribution of waves varies with time. When the ground is natural, the dynamic waves can propagate continuously all the time. However, when the SMM is adopted, the dynamic waves change their propagation paths due to the barriers. The accelerations in the SMM area and at the right-back of SMM area exhibit noticeable vibration shielding effects.

5.2.2 Frequency domain analysis

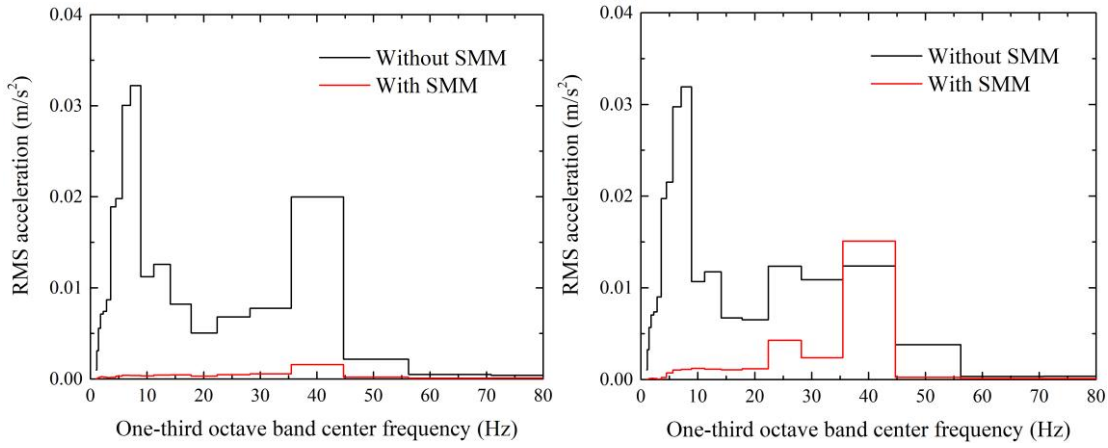

(a) (b)

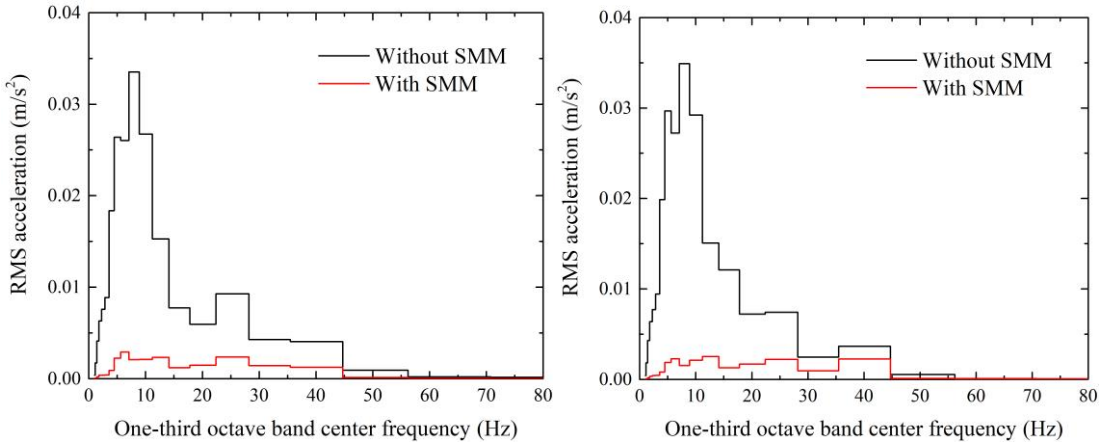

(c) (d)

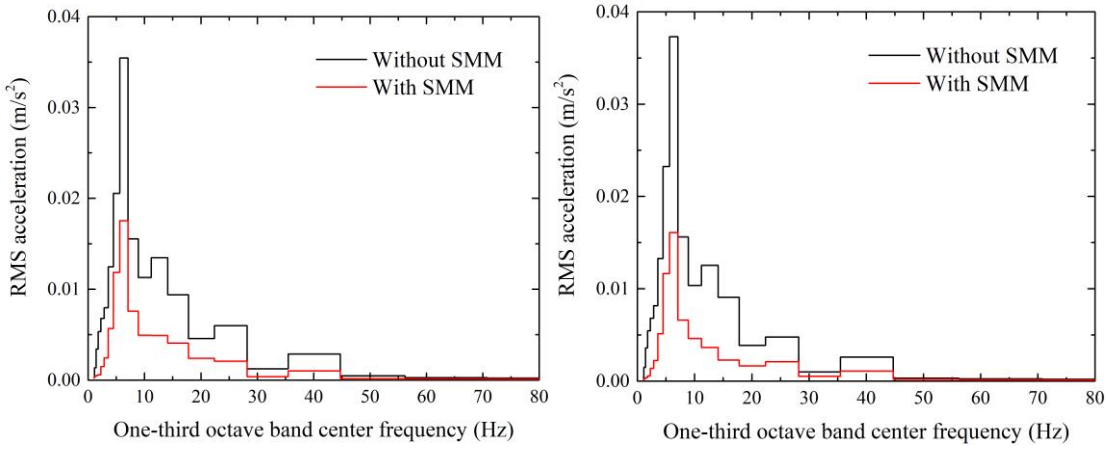

(e) (f)

Figure 12 One-third octave band RMS spectrum of the acceleration level of ground (a) Point A (b) Point B (c) Point C (d) Point D (e) Point E (d) Point F

The root mean square (RMS) acceleration is an important indicator to evaluate the vibration level. The time histories of the ground vibration acceleration at a one-third octave band are obtained by conducting the filter processing to the frequency components. And the one-third octave band RMS spectrum can be calculated as follows:

$$a_{rms} = \sqrt{\lim_{N_s \to \infty} \frac{1}{N_s} \sum_{k=0}^{N_s} [a_w(k)]^2} \tag{8}$$

where $a_w(k)$ is the discrete-time history of acceleration at a one-third octave band, and N_s is the sampling number.

The one-third octave band RMS spectrum at six key points are shown in Figure 12. The SMM exhibits excellent ground vibration mitigation effects in frequency domain. When the ground is natural, the pronounced frequency components are around 8 Hz and 40 Hz at Point A and B, but the frequency component of 8 Hz is significantly reduced when the SMM is adopted, as shown in Figure 12 (a) and (b). A similar reduction effect by using SMM can be observed for Point C, D, E and F. Since the theoretical band gap is 0-9.1 Hz, the dispersion relation predicts the attenuation frequency bands quite well. It is also noted that the reduction components are not only the pronounced component of 8 Hz but also the frequencies with a relatively large band (around 0-45 Hz), indicating that SMM could have a better mitigation effect in reality than theoretical predictions from dispersion analysis.

To quantify how much the acceleration level has been reduced due to the SMM in the

one-third octave band RMS spectrum, the insertion loss (IL) from the ratio of the RMS acceleration of the ground without and with SMM is calculated as follows:

$$\mathrm{IL} = 20 \cdot \lg \frac{a_{\text{without}}}{a_{\text{with}}} \tag{9}$$

where a_{without} is the RMS acceleration of the ground without SMM, and a_{with} denotes the RMS acceleration of the ground with SMM. Positive values indicate a significant reduction of vibration level, while negative values correspond to an inverse amplification effect using SMM.

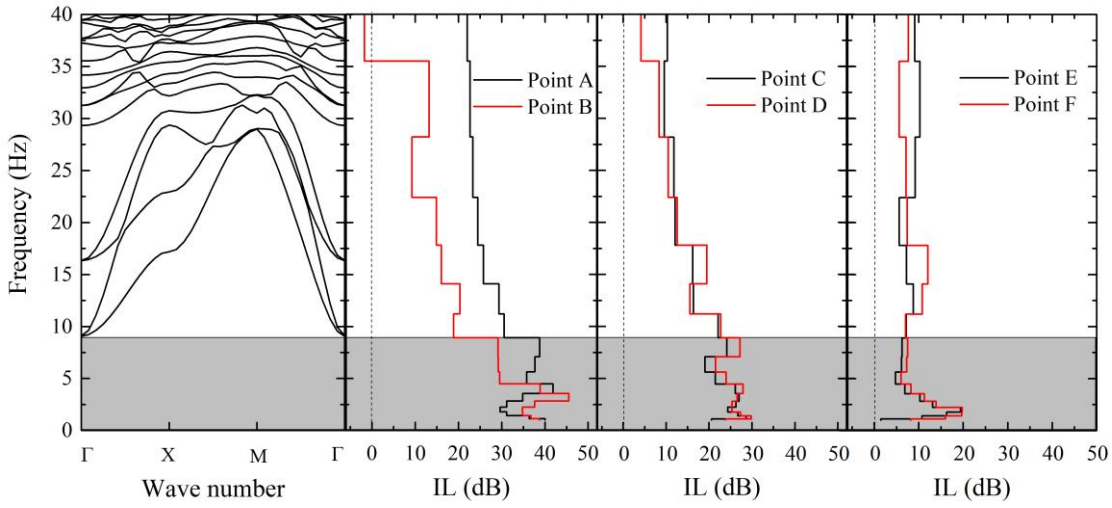

Figure 13 Insertion loss (a) Theoretical band gap (b) IL at Point A and B (c) IL at Point C and D (d) IL at Point E and F

Figure 13 illustrates the IL at six key points when they are compared with the theoretical band gap. The SMM can reduce the vibration level with an IL of around 45 dB at 24.4 m (Point A and B). The maximum IL is 30 dB and 20 dB at 30 m (Point C and D) and 36.4 m (Point E and F), respectively. Therefore, the maximum mitigation effect reduces with the three distances. The IL shows its maximum values at frequencies of 0-9.1 Hz, which corresponds to the theoretical band gap. In addition, the SMM also globally exhibits good vibration mitigation effect when frequencies are lower than 40 Hz.

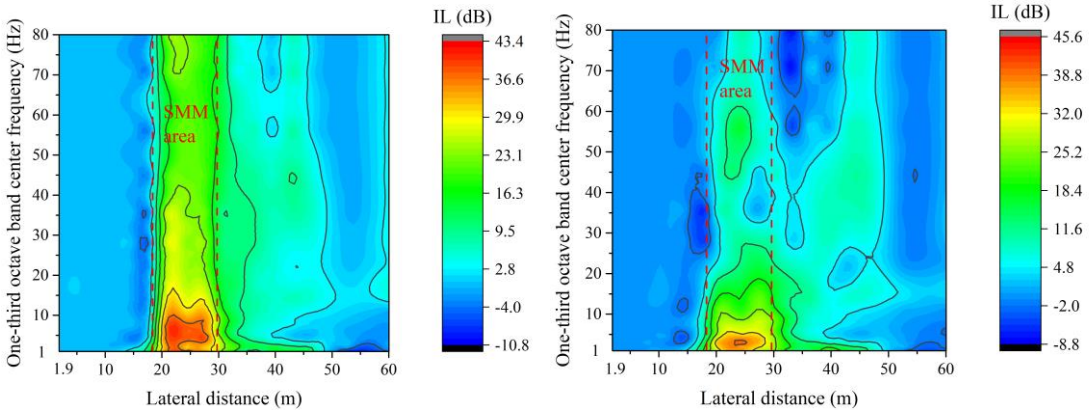

(a) (b)

Figure 14 Insertion loss (a) Line I (b) Line II

The IL along with two lines are shown in Figure 14. The maximum IL occurs in the SMM area at frequencies lower than 9 Hz, indicating the SMM performs a significant vibration attenuation effect. The two lines show a similar phenomenon referring to the IL, but the maximum IL has small differences (43.3 dB for Line I, and 45.6 dB for Line II).

6. Parametric studies

In order to obtain a comprehensive knowledge of the ground vibration mitigation using SMM in railways, the number of inclusions, the initial distances of the SMM, and the train speeds are changed to investigate their influences on the attenuation effects.

6.1 Number of inclusions

The number of inclusions is chosen as 2×2, 4×4, and 6×6. The distribution of different numbers of inclusions can be seen from Figure 8. Figure 15 shows the ground vibration mitigation results under three cases.

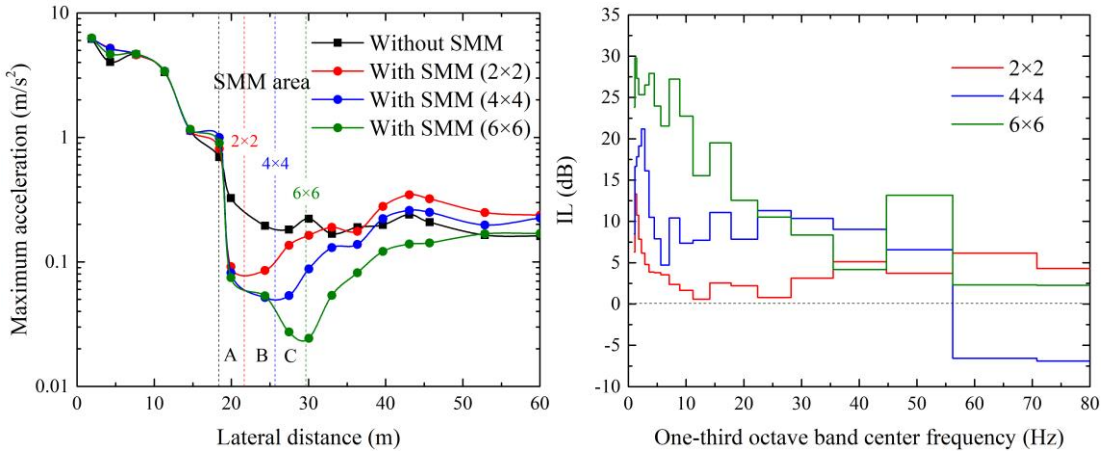

(a) (b)

Figure 15 Ground vibration responses with different numbers of inclusions (a) Maximum acceleration along with Line II (b) Insertion loss at Point D

As shown in Figure 15 (a), the region A represents that the positions are located in SMM area for all three cases (2×2, 4×4, and 6×6, red square in Figure 8). The positions in region B are in SMM area for two cases (4×4, and 6×6, blue square in Figure 8), and points in region C are only in SMM area with 6×6 inclusions (Green square in Figure 8). In all three cases, the mitigation effect appears when the dynamic waves approach the SMM area. In region A, the values of attenuated accelerations are quite similar for three cases. In region B, the accelerations in the case of 4×4 inclusions are lower than those of 2×2 inclusions, but they are identical with those of 6×6 inclusions. In region C, the case of 6×6 inclusions exhibits the best mitigation effect. Therefore, no matter the number of inclusions, the SMM has similar mitigation acceleration values as long as the locations are within the area of periodic barriers. When the distance overtakes the back edge of the SMM area, the accelerations are recovered, and the values can be higher than those of natural ground.

The IL with cases of 2×2, 4×4, and 6×6 inclusions is shown in Figure 15 (b). The case of 6×6 inclusions has maximum IL with 30 dB, while the case of 4×4 inclusions exhibits 23 dB, and the 2×2 inclusions can reduce the vibration level with 13 dB. Therefore, when frequencies are lower than 45 Hz, the mitigation of ground vibration level is significant with increasing the number of inclusions. Also, the maximum values of IL occur at frequencies lower than 9 Hz for three cases, corresponding to the theoretical dispersion prediction. It is also noted that the case of 4×4 inclusions exhibits negative values of IL when the frequencies

are higher than 55 Hz, indicating that the vibration level can be amplified due to the propagations of dynamic waves behind the SMM area.

6.2 Initial distance

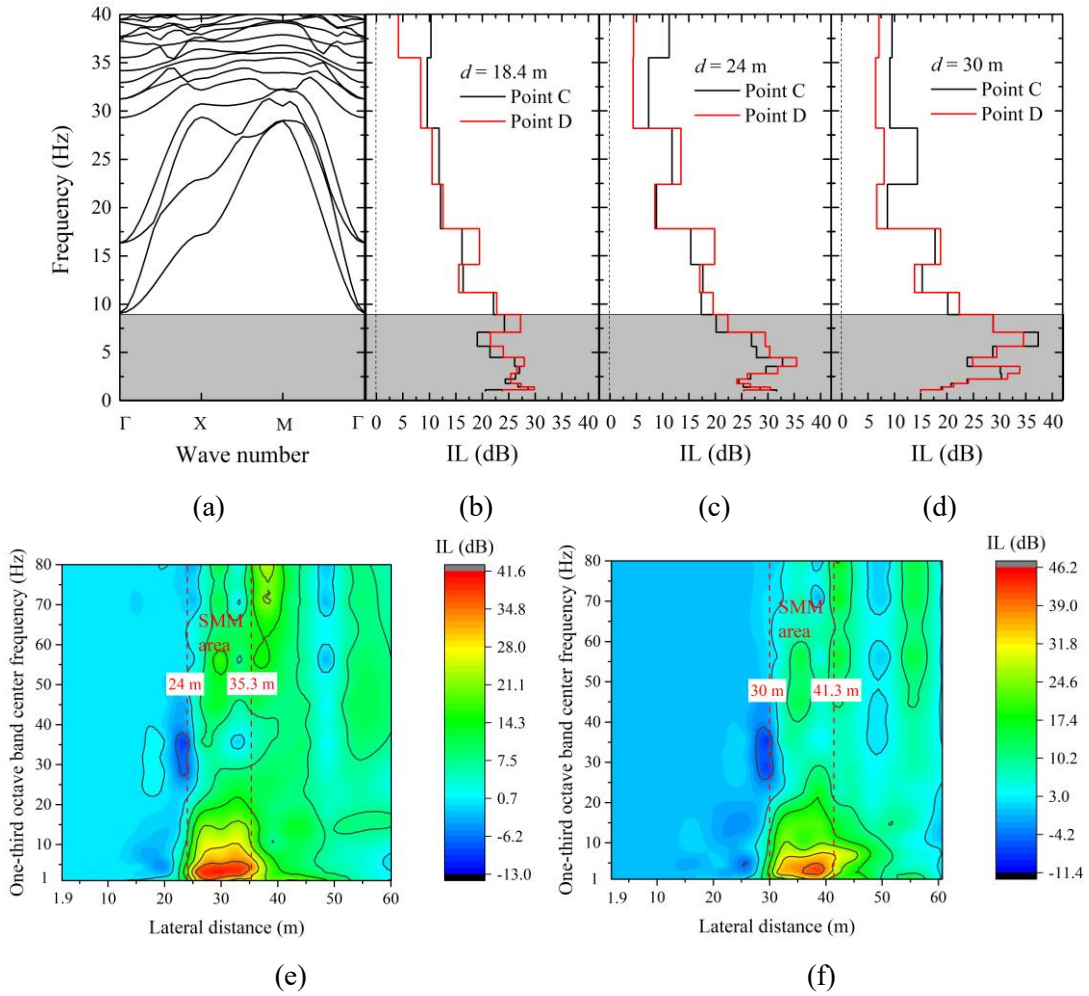

Figure 16 Insertion loss with different initial distances (a) theoretical band gap (b) IL at two points when d =18.4 m (c) IL at two points when d = 24 m (d) IL at two points when d = 30 m (e) IL distribution with Line II when d = 24 m (f) IL distribution with Line II when d = 30 m

The initial distance (d, as shown in Figure 8) between the front edge of the SMM and the center line of the track is varied for 18.4 m, 24 m and 30 m. Figure 16 shows the IL with three cases. Note that Point C and D are relative positions to the SMM area in Figure 16 (b), (c) and (d). When d =18.4 m, $d_{C/D}$=30 m; When d =24 m, $d_{C/D}$=35.6 m; and when d =30m, $d_{C/D}$= 41.6 m. The IL at Point C and D exhibit a similar tendency for three cases. Although the maximum values of IL have some differences, they occur at the frequencies of 0-9.1 Hz. The

IL distribution can also reflect the SMM locations since the maximum IL appears in SMM area, as shown in Figure 16 (e) and (f). Therefore, the initial distance exhibits an insignificant influence on the ground vibration mitigation effect using SMM.

6.3 Train speed

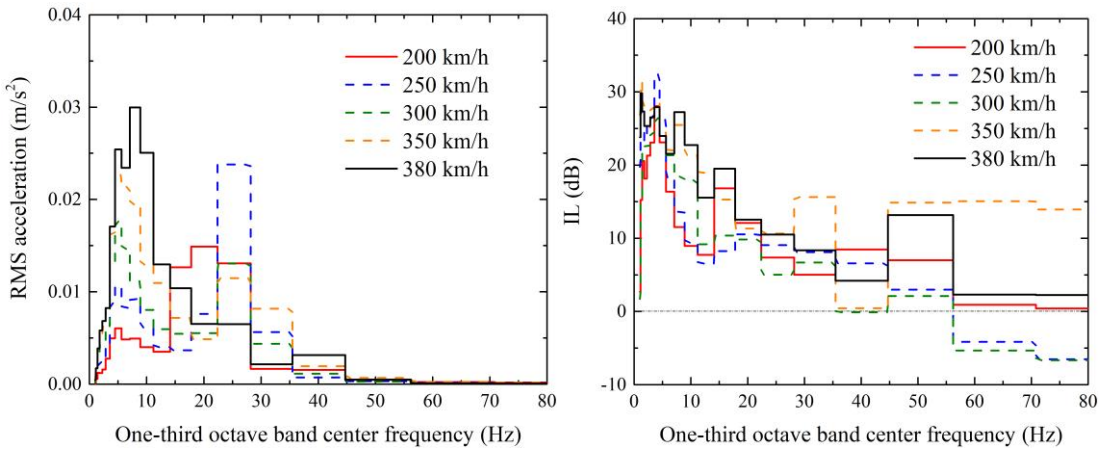

(a) (b)

Figure 17 Ground vibration responses with varied train speeds (a) One-third octave band RMS spectrum of ground without SMM at Point D (b) IL at Point D

The train speed is changed from 200 km/h to 380 km/h. Since the frequency components of ground can change with train speed, the one-third octave band RMS spectrum of natural ground is first obtained with five cases of train speeds, as shown in Figure 17 (a). When the train speed is relatively lower (200 km/h and 250 km/h), the pronounced frequencies are distributed in 20-30 Hz. When the train speed is higher (≥300 km/h), the frequency components within 9 Hz are more evident. Figure 17 (b) shows the corresponding IL with different train speeds. Although the significant frequency components change with train speeds, the mitigation of ground vibration level is still pronounced within frequencies lower than 9 Hz since the band gap is one of the inherent characteristics of the SMM. It is noted that the distribution of IL is scattered with different train speeds when the frequencies are higher than 40 Hz, but it is insignificant since the RMS accelerations are quite low at these frequencies.

7. Conclusions

As an innovative vibration mitigation solution, seismic metamaterial (SMM) has received increasing attention as it can theoretically shield dynamic waves in certain frequency bands. However, the application of the SMM in railways is recent, and the related research is ongoing, so the mitigation effects by SMM in railway-induced ground vibrations are still unknown. This study is thus the world's first to investigate the ground vibration mitigation using SMM-based barriers in high-speed railways. The dispersion theory is proposed to obtain the theoretical band gaps of the SMM. In order to investigate the influence of SMM on the ground vibrations, a 3D coupled train-track-soil model is developed based on the multi-body simulation principle, finite element theory and perfectly matched layers method using LS-DYNA. The proposed models were validated by comparing the results with previous works. Based on the ground vibration responses from the models with and without SMM, the following conclusions can be drawn:

(a) The pronounced frequency components should be attenuated in railways, and they correspond to the theoretical band gap of SMM. Although the dominant frequencies of natural ground vary with the distance from the railway track, they are lower than 9 Hz at longer distances in this study. The SMM, which is adopted in this railway, possesses a band gap with 0 - 9.1 Hz.

(b) In time domain, the SMM performs an excellent vibration mitigation effect. The mitigation of acceleration occurs both in and behind the SMM area. The accelerations reduce by a maximum of 96%. Also, the SMM interferes with the propagation paths of dynamic waves and attenuates the vibration accelerations.

(c) In frequency domain, the most significant vibration mitigation components in railways correspond to the theoretical dispersion predictions, which is lower than 9 Hz. However, the SMM globally exhibits a better mitigation effect in railways. The SMM can significantly reduce the ground vibration level since the maximum insertion loss is higher than 40 dB.

(d) The number of inclusions can increase the mitigation effect of SMM, while the initial distance of SMM exhibits an insignificant impact on ground vibrations. In addition, the train

speed can arouse different pronounced frequency components, but the mitigation components are still determined based on the dispersion relations. Therefore, when the SMM is adopted in railways, the number of inclusions and train speed should be considered in practice.

It is also noted that this study aims to create new contribution towards a better understanding into the mitigation effects by SMM for railway-induced ground vibrations. This simulation can reflect the vibration mitigation effect using SMM to a certain extent. Further experimental studies are recommended to be investigated in the future before the SMM is adopted in railways in practice.

Acknowledgments

This research was supported by the Key Research Development Program of China (No.2016YFC0802203-2, No.2016YFC0802203-3). The authors sincerely thank European Commission for H2020-MSCA-RISE Project No. 691135 "RISEN: Rail Infrastructure Systems Engineering Network," which enables a global research network that tackles the grand challenge in railway infrastructure resilience and advanced sensing under extreme conditions (www.risen2rail.eu) [38].

References

[1] Connolly DP, Marecki GP, Kouroussis G, Thalassinakis I, Woodward PK. The growth of railway ground vibration problems - A review. Science of the Total Environment. 2016;568:1276-82.

[2] Remennikov AM, Kaewunruen S. A review of loading conditions for railway track structures due to train and track vertical interaction. Struct Control Health Monit. 2008;15(2):207-34.

[3] Zhai WM, Han ZL, Chen ZW, Ling L, Zhu SY. Train-track-bridge dynamic interaction: a state-of-the-art review. Vehicle System Dynamics. 2019;57(7):984-1027.

[4] Li T, Su Q, Kaewunruen S. Influences of piles on the ground vibration considering the train-track-soil dynamic interactions. Computers and Geotechnics. 2020;120:12.

[5] Li T, Su Q, Kaewunruen S. Saturated Ground Vibration Analysis Based on a Three-Dimensional Coupled Train-Track-Soil Interaction Model. Appl Sci-Basel. 2019;9(23):18.

[6] Li ZG, Wu TX. On vehicle/track impact at connection between a floating slab and ballasted track and floating slab track's effectiveness of force isolation. Vehicle System Dynamics. 2009;47(5):513-31.

[7] Sol-Sanchez M, Moreno-Navarro F, Rubio-Gamez MC. The use of elastic elements in railway tracks: A state of the art review. Construction and Building Materials. 2015;75:293-305.

[8] Connolly D, Giannopoulos A, Fan W, Woodward PK, Forde MC. Optimising low acoustic impedance back-fill material wave barrier dimensions to shield structures from ground borne high speed rail vibrations. Construction and Building Materials. 2013;44:557-64.

[9] Thompson DJ, Jiang J, Toward MGR, Hussein MFM, Ntotsios E, Dijckmans A, et al. Reducing railway-induced ground-borne vibration by using open trenches and soft-filled barriers. Soil Dynamics and Earthquake Engineering. 2016;88:45-59.
[10] Pu XB, Shi ZF. Surface-wave attenuation by periodic pile barriers in layered soils. Construction and Building Materials. 2018;180:177-87.
[11] Colombi A, Roux P, Guenneau S, Gueguen P, Craster RV. Forests as a natural seismic metamaterial: Rayleigh wave bandgaps induced by local resonances. Sci Rep. 2016;6:7.
[12] Muhammad, Lim CW, Reddy JN. Built-up structural steel sections as seismic metamaterials for surface wave attenuation with low frequency wide bandgap in layered soil medium. Engineering Structures. 2019;188:440-51.
[13] An XY, Fan HL, Zhang CZ. Elastic wave and vibration bandgaps in two-dimensional acoustic metamaterials with resonators and disorders. Wave Motion. 2018;80:69-81.
[14] Brule S, Enoch S, Guenneau S. Emergence of seismic metamaterials: Current state and future perspectives. Phys Lett A. 2020;384(1):11.
[15] Peng H, Pai PF. Acoustic metamaterial plates for elastic wave absorption and structural vibration suppression. Int J Mech Sci. 2014;89:350-61.
[16] Kaewunruen S, Martin V. Life Cycle Assessment of Railway Ground-Borne Noise and Vibration Mitigation Methods Using Geosynthetics, Metamaterials and Ground Improvement. Sustainability. 2018;10(10):21.
[17] Chen YY, Qian F, Scarpa F, Zuo L, Zhuang XY. Harnessing multi-layered soil to design seismic metamaterials with ultralow frequency band gaps. Mater Des. 2019;175:8.
[18] Achaoui Y, Antonakakis T, Brule S, Craster RV, Enoch S, Guenneau S. Clamped seismic metamaterials: ultra-low frequency stop bands. New J Phys. 2017;19:13.
[19] Huang JK, Liu W, Shi ZF. Surface-wave attenuation zone of layered periodic structures and feasible application in ground vibration reduction. Construction and Building Materials. 2017;141:1-11.
[20] Huang JK, Shi ZF. Attenuation zones of periodic pile barriers and its application in vibration reduction for plane waves. Journal of Sound and Vibration. 2013;332(19):4423-39.
[21] Krodel S, Thome N, Daraio C. Wide band-gap seismic metastructures. Extreme Mech Lett. 2015;4:111-7.
[22] Ungureanu B, Achaoui Y, Enoch S, Brule S, Guenneau S. Auxetic-like metamaterials as novel earthquake protections. EPJ Appl Metamaterials. 2016;2:8.
[23] Brule S, Javelaud EH, Enoch S, Guenneau S. Experiments on Seismic Metamaterials: Molding Surface Waves. Phys Rev Lett. 2014;112(13):5.
[24] Brule S, Javelaud EH, Enoch S, Guenneau S. Flat lens effect on seismic waves propagation in the subsoil. Sci Rep. 2017;7:9.
[25] Miniaci M, Krushynska A, Bosia F, Pugno NM. Large scale mechanical metamaterials as seismic shields. New J Phys. 2016;18:14.
[26] Meng LK, Cheng ZB, Shi ZF. Vibration mitigation in saturated soil by periodic pile barriers. Computers and Geotechnics. 2020;117:9.
[27] Thompson DJ, Kouroussis G, Ntotsios E. Modelling, simulation and evaluation of ground vibration caused by rail vehicles. Vehicle System Dynamics. 2019;57(7):936-83.
[28] Shi ZF, Chen ZB; Xiang HJ. Periodic structures: Theory and Applications to seismic isolation and vibration reduction. Beijing. 2017.

566 [29] Pu XB, Shi ZF. A novel method for identifying surface waves in periodic structures. Soil
567 Dynamics and Earthquake Engineering. 2017;98:67-71.
568 [30] Wang MZ, Cai CB, Zhu SY, Zhai WM. Experimental study on dynamic performance of typical
569 nonballasted track systems using a full-scale test rig. Proc Inst Mech Eng Part F-J Rail Rapid Transit.
570 2017;231(4):470-81.
571 [31] Lei XY, Wang J. Dynamic analysis of the train and slab track coupling system with finite elements
572 in a moving frame of reference. Journal of Vibration and Control. 2014;20(9):1301-17.
573 [32] Basu U. Explicit finite element perfectly matched layer for transient three-dimensional elastic
574 waves. International Journal for Numerical Methods in Engineering. 2009;77(2):151-76.
575 [33] Wang J, Jin X, Cao Y. High-speed maglev train-guideway-tunnel-soil modelling of ground
576 vibration. Proc Inst Mech Eng Part F-J Rail Rapid Transit. 2012;226(F3):331-44.
577 [34] Kouroussis, G., Connolly, D. P., Verlinden, O. Railway-induced ground vibrations–a review of
578 vehicle effects. International Journal of Rail Transportation, 2014, 2(2), 69-110.
579 [35] Kaewunruen, S., Remennikov, A.M. Current state of practice in railway track vibration isolation:
580 an Australian overview, Australian Journal of Civil Engineering, 2016, 14:1, 63-71, DOI:
581 10.1080/14488353.2015.1116364
582 [36] Ngamkhanong, C., Kaewunruen, S., The effect of ground borne vibrations from high speed train
583 on overhead line equipment (OHLE) structure considering soil-structure interaction, Science of The
584 Total Environment, 2018, 627, 934-941.
585 [37] Ngamkhanong C, Kaewunruen S and Baniotopoulos C (2018) Far-Field Earthquake Responses of
586 Overhead Line Equipment (OHLE) Structure Considering Soil-Structure Interaction. Front. Built
587 Environ. 4:35. doi: 10.3389/fbuil.2018.00035
588 [38] Kaewunruen S, Sussman JM and Matsumoto A (2016) Grand Challenges in Transportation and
589 Transit Systems. *Front. Built Environ.* 2:4. doi: 10.3389/fbuil.2016.00004
590